

# Nanoscale

Accepted Manuscript



This is an *Accepted Manuscript*, which has been through the Royal Society of Chemistry peer review process and has been accepted for publication.

*Accepted Manuscripts* are published online shortly after acceptance, before technical editing, formatting and proof reading. Using this free service, authors can make their results available to the community, in citable form, before we publish the edited article. We will replace this *Accepted Manuscript* with the edited and formatted *Advance Article* as soon as it is available.

You can find more information about *Accepted Manuscripts* in the [Information for Authors](#).

Please note that technical editing may introduce minor changes to the text and/or graphics, which may alter content. The journal's standard [Terms & Conditions](#) and the [Ethical guidelines](#) still apply. In no event shall the Royal Society of Chemistry be held responsible for any errors or omissions in this *Accepted Manuscript* or any consequences arising from the use of any information it contains.

## ARTICLE

## Material effects on V-nanoantenna performance

Cite this: DOI: 10.1039/x0xx00000x

S. K. Earl,<sup>a,b</sup> D. E. Gomez,<sup>b,c</sup> T. D. James,<sup>a,b</sup> T. J. Davis<sup>b,c</sup> and A. Roberts<sup>a</sup>Received 00th January 2012,  
Accepted 00th January 2012

DOI: 10.1039/x0xx00000x

www.rsc.org/

There is great interest in aluminum based plasmonic devices due to the relatively high plasma frequency of this material as well as its low cost and self-passivating oxide layer. The passivation layer provides aluminum plasmonics with the long-term stability required for practical applications. While several studies have investigated the impact of this oxide layer on the plasmon resonances of aluminum nanostructures on glass substrates, little is known about the effect of high-refractive index substrates on these resonances. Here we present an investigation of aluminum V-shaped antennas resonant in the visible on a silicon substrate. Through comparison between numerical and experimental results, we show that the aluminium passivation layer has little effect on the antenna resonances by comparing numerical simulations both with and without. We show, however, that inclusion of the native oxide layer of the silicon substrate in numerical models is critical for achieving good agreement with experimental data. Furthermore, we computationally explore the influence of the 1.5 eV interband transition of aluminum on plasmon resonances, and find that its effect on the material properties of the resonant structures results in narrower resonances in the blue part of the spectrum than if it was not present.

## Introduction

Optical antennas are nanostructures that can efficiently couple far- to near-field radiation (and vice-versa).<sup>1</sup> Here we use localized surface plasmons (LSPs) in metallic nanoparticles to manipulate light in the optical near-field at dimensions far below that of diffractive optics.<sup>2</sup> There are, however, significant gaps in our understanding of the way these plasmonic nanostructures behave. One important phenomenon yet to be fully understood is the influence of optically-dense materials in the near field region of resonant structures, most notably the effect of high refractive index substrates supporting metallic nanostructures. The issue of high index substrates is of great importance to the potential integration of plasmonic structures with current silicon-based technologies,<sup>3</sup> tunable plasmonics enabled by active materials<sup>4</sup> and the incorporation of plasmonic structures with metal oxides (hematite, TiO<sub>2</sub>, etc) for enhancing their photo-catalytic efficiency.<sup>5,6</sup>

Particles on substrates with high refractive indices display a red-shift in their resonance frequencies.<sup>7</sup> The influence of the substrate in producing this red-shift has been successfully explained through the introduction of induced image charges at the interface between the sub- and super-strates.<sup>8-10</sup> It has also been shown that the substrate splits the degeneracy of the dipole plasmon modes oriented parallel and perpendicular to the substrate surface<sup>11</sup>, an effect that was found to depend heavily on substrate permittivity. Particles on substrates are in vertically-asymmetric environments, which can lead to mixing or interactions between different plasmon modes of the antennas leading to the observed red-shift, breaking of degeneracies<sup>12</sup> and Fano-type line shapes<sup>13</sup> in the scattering

spectra. This is due to the hybridization of the modes of the particle and its image charge within the substrate.<sup>14</sup>

The hybridization effect is best understood directly through the inspection of numerically simulated field and surface charge distributions, and indirectly observed experimentally via scattering spectra. The finite-difference time-domain (FDTD) method has been used to show the effect of a substrate on the plasmonic resonances of a nano-cube,<sup>15</sup> finding that additional resonances appeared as the cube approached the substrate. A similar result was shown for silver nanoparticles on a range of substrates with different refractive indices.<sup>7</sup> Numerical simulations were also used to study a nano-cube (Ag) near substrates with permittivities of 2.25 (glass) and 7.5 (ZnSe),<sup>12</sup> showing the previously mentioned red-shift of the dipole mode and the introduction of extra resonances as the particle-substrate distance decreased. A recent experiment investigated the visible and near-IR behavior of Al rod arrays on KTaO<sub>3</sub>,<sup>16</sup> with a refractive index of 2.21, but many materials, such as silicon, display a much higher refractive index within the visible wavelengths.

Reducing the thickness of the substrate has been shown to blue-shift the LC resonance of THz split-ring resonators on silicon substrates.<sup>17</sup> Yang *et al.*<sup>18</sup> also observed that for silicon substrates the plasmonic resonances of a silver nanoparticle were extremely sensitive to substrate thickness in the visible range. This was a clear demonstration of the effect a substrate can have on the resonances of a structure placed on it. Numerical and theoretical investigations have shown that arrays of resonant apertures in metal films are similarly affected.<sup>19-21</sup>

An understanding of the effect of a dense substrate on plasmonic nanostructure resonances has significant

implications for applications such as sensing<sup>17, 22</sup> and communications<sup>23</sup> through enabling the manipulation of higher-order resonances and simplifying the integration of plasmonic devices into silicon-based circuits. An additional, and important, motivator for this work is that improved understanding of plasmonic resonances on high-index semiconductors will enable the increase in efficiency of plasmonically-enhanced photocatalysis structures<sup>24</sup>.

While gold and silver have traditionally been used to create optical antennas, recent research has explored alternative materials.<sup>25</sup> Aluminum is emerging as a promising candidate to replace noble metals due to its high plasma frequency and self-passivating oxide layer.<sup>26-31</sup> Its high plasma frequency, which produces shorter-wavelength plasmonic resonances than otherwise identical structures fabricated using other metals,<sup>27</sup> has the potential to compensate for the red-shift caused by the proximity of a dense substrate. The well-documented passivation properties of aluminum,<sup>26, 31</sup> even on the nanoscale, are also favorable for device longevity.

In this work we investigate the effect of an optically-dense silicon substrate on the modes of an aluminum V-shaped antenna. The V-antenna geometry was chosen for its single plane of symmetry and because it can be designed to display two non-degenerate dipolar resonances.<sup>32</sup> Through examination of the extent of the agreement between experimental and numerical results we show that it is necessary to include the native oxide present on the silicon substrate, however, the ultra-thin oxide layer on the aluminum antennas does not need to be included in the model to achieve good agreement between simulated and experimental results.<sup>31</sup> We use the V-antenna design to numerically explore the influence of the aluminum's interband transition on the antennas, finding that, as expected, it has a strong impact upon the resonances of the structure. Finally, through inspection of the structure's surface charge distributions, calculated via the finite element method (FEM), we show a significant difference between those of single, isolated antennas and those in an array, indicating that adjacent antennas are affecting the nature of the resonant mode.

### Fabrication

The substrates used were 4" p-doped, (100) orientated silicon wafers. The wafers were spin-coated with a dual resist coating of Methyl Methacrylate / (Poly) Methyl Methacrylate (MMA/PMMA) to an approximate combined thickness of 250 nm. The PMMA-A2 provides a high resolution layer while the MMA-EL6 undercuts, producing vertical side walls and aiding liftoff. Electron Beam Lithography (EBL) was performed with a Vistec EBPG 5000 tool with a 100 kV source and a 200 pA beam with a 200  $\mu\text{m}$  aperture. The structures, written with a range of doses from 800  $\mu\text{C}/\text{cm}^2$  to 1500  $\mu\text{C}/\text{cm}^2$ , were V-antennas with an interior flare angle of 80 degrees with arms 30 nm wide and 100 nm long, as measured from the outside, in square arrays of 200  $\mu\text{m}$  per side with a period of 250 nm.

Following the EBL process, the wafer was developed in a 1:3 mix of Methyl Isobutyl Ketone : Isopropyl Alcohol (MIBK:IPA) to remove the exposed resist. A 5 minute argon plasma clean was then followed by the evaporation of a 40 nm thick layer of aluminum at  $2 \times 10^{-6}$  Torr (deposition rates of 0.025 nm/s and then 0.1 nm/s). Lift-off was performed using agitation in a warm (60 °C) bath of acetone, followed by rinsing in separate room temperature acetone, IPA and de-ionized water baths before being dried with pure nitrogen gas. Upon completion of lift-off the sample was imaged using a scanning electron microscope (SEM). Fig. 1(a) presents an SEM image

of the V-antenna arrays. Some variation in antenna shape across the arrays was observed, mainly in relation to the inner corner of the V and the symmetry of the structure. It would be reasonable to expect some broadening of the optical response from the array as a result, although the numerical simulations presented still agree well with experimental measurements (see discussion section).

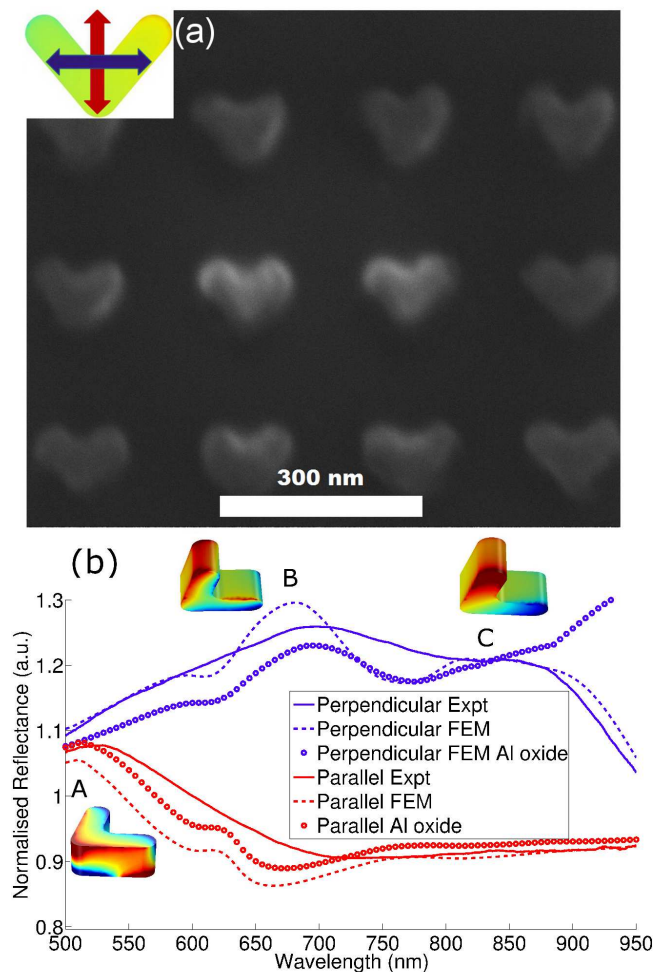


**Fig. 1** (a) SEM image of V-antenna array, taken in BSE mode; (inset) definition of excitation polarization relative to the symmetry axis of the V-antenna, colour-coded to the accompanying plot; (b) Normalised reflectance from aluminum V-antenna array on silicon substrate with 3 nm intervening native oxide. Experimental (solid lines) and numerical (dotted lines indicate inclusion of 3 nm SiO<sub>2</sub> on substrate while circles indicate inclusion of 3 nm SiO<sub>2</sub> on substrate and 3 nm of Al<sub>2</sub>O<sub>3</sub> on air-facing surfaces of antenna) data show the reflection normalised to that of the adjacent substrate; greater than 1 indicates an increase in reflection over that of the substrate alone; (inset, upper) surface charge distributions at 680 nm and 850 nm for perpendicular excitation; (inset, lower) surface charge distribution at 510 nm for parallel excitation. The red and blue coloration indicates regions of opposite charge, while green indicates a neutral region. Surface charge plots relate to the dotted line FEM plots.

### Spectroscopy

Normal incidence spectroscopy was used to characterize the optical behavior of the arrays, enabling simple comparison with

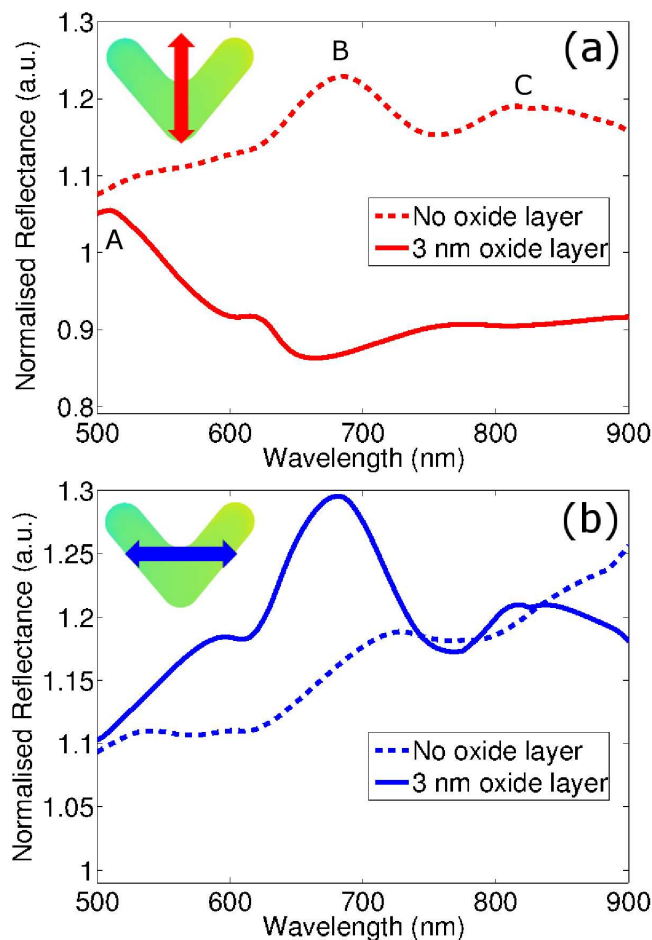
numerical modeling as discussed later. A fibre-coupled halogen white light source (HL-2000-FHSA) was collimated using a 10x, 0.4 NA lens (Olympus UPlan SApo) and polarised with a linear polariser (Thorlabs LPVIS050-MP, 550-1.5  $\mu\text{m}$ ) before being directed through a beam splitter (Thorlabs CM1-BS013, 400-700 nm). After the beam splitter a 20x, 0.4 NA lens (Olympus Plan N) focused the light onto the sample at normal incidence, resulting in a focused spot of approximately 2.5  $\mu\text{m}$ . Reflection from the sample was collected using the same lens and out-coupled through the beam splitter to a lens which focused the beam onto the end of a fibre-coupled spectrometer (Ocean Optics QE65000) connected via USB to a computer. Array reflection measurements were normalised to the reflection of the adjacent substrate and are shown in Fig. 1(b), along with results of numerical modeling (discussed in the following section). Reflectivity data is presented as  $R_e = R_{\text{sample}}/R_{\text{substrate}}$ , where  $R_{\text{sample}}$  is the reflectivity measured on the antenna arrays while  $R_{\text{substrate}}$  corresponds to that of the bare substrate immediately adjacent to the arrays. Therefore,  $R_e$  can have values greater than one, indicating enhanced reflectance.

## Discussion

To understand the nature of the resonances of the V-antennas the FEM package COMSOL Multiphysics 4.3a was used to simulate an identical array. Periodic boundary conditions were used in the x- and y-directions to simulate an infinite array; while the fabricated array is finite, it is sufficiently larger than the spot used to excite the array to avoid any edge effects. A scattering boundary was used on the lower boundary to prevent reflections and a port boundary condition was used on the upper boundary to both excite the unit cell and absorb any reflections. This was sufficient, since only normally-incident light was used and the period is such that only the zeroth-order was reflected. The dielectric material properties of silicon, aluminum oxide and aluminum were obtained from the results of Palik<sup>33</sup> and Rakic<sup>34</sup>. The native oxide typically present on silicon wafers was included in the simulations as an intervening 3 nm  $\text{SiO}_2$  layer between the V-antenna and the silicon. A refractive index of 1.45 was used for this layer. Materials data used in simulations was that of a bulk materials; thin films on the nanoscale are known to vary significantly from bulk due to deposition method, environment and granularity. This accounts for much of the small variation between experimental and numerical data shown in Fig. 1(b). The other main source of this discrepancy is unavoidable variations between the precise geometry of individual nanostructures. Small variances in the exact geometry of the metallic nanostructures will broaden and weaken the experimental peaks of the arrays, as the measured spectra are averages of many thousands of antenna.

Inspection of Fig. 1(b) shows that the inclusion of the aluminum oxide layer on the outer surfaces of the V-antenna actually reduces the overall agreement between simulation and experiment. While the main plasmon resonance peak wavelengths display a slightly improved agreement (on the order of 10 nm), a large disparity at longer wavelengths is observed. In the numerical model the presence of the aluminum oxide on the particle has the effect of red-shifting the plasmon resonance (dielectric red-shift, a well-known phenomenon) as well as blue-shifting it (by shortening the resonant length of the metallic structure). However, the presence of the optically-dense silicon appears to minimize both these effects, enabling accurate simulation of the normalized reflection spectrum without inclusion of the metal oxide. We hypothesize this is due to the resonances' localization to the substrate surface, as

shown in the insets of Fig. 1(b). For sufficient localization to the substrate the resonance would be far enough from any metal oxide its influence would be weak enough to be omitted from simulations in the interest of computational efficiency while still producing strong agreement with experiment. Due to this, simulations for the remaining portion of the paper therefore omit the aluminum oxide but retain the  $\text{SiO}_2$  on the substrate.



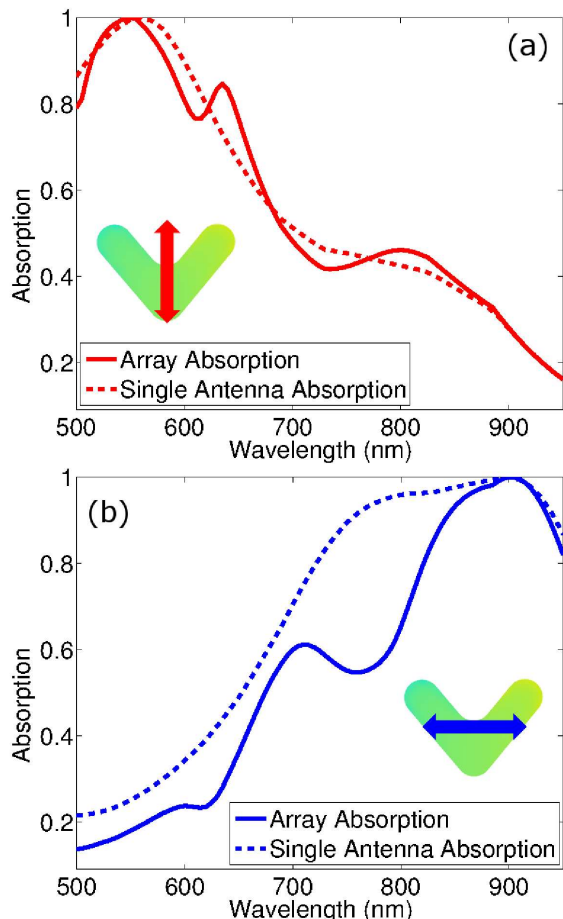
**Fig. 2** Simulated normalised reflectance from the Al antenna arrays on silicon (dotted) and silicon with a 3 nm native oxide layer (solid) for (a) parallel and (b) perpendicular excitation, defined as indicated by the insets.

Fig. 2 shows a comparison of the normalised reflectance from the simulated array both with (solid line) and without (dotted line) the native oxide layer. It clearly shows that inclusion of the silicon substrate's native oxide layer within the numerical model is necessary to achieve agreement with experimental results, as shown in Fig. 1(b). The disparity between the two cases (3 nm oxide versus no oxide layer) is unsurprising considering the location of the oxide layer is where the resonant field is most intense, in the near-field of the antennas exhibiting a resonance. At resonance, the electric field is highly localized around the particle, and as such is heavily influenced by its local dielectric environment. By preventing direct contact between the antennas and the much denser silicon, the oxide layer significantly reduces the exposure of the resonant fields to the underlying silicon, thereby reducing the red-shift of the resonance. Careful manipulation of the underlying  $\text{SiO}_2$  layer's thickness could be used in this way to fine tune the plasmon resonance of a structure it supported, however the tuning

mechanism would be extremely sensitive to small variations in the layer thickness and therefore difficult to apply.

The impact of the aluminum interband transition around 800 nm is also highlighted in Fig. 2 through its effect on the reflection spectra of the antenna arrays. It can be seen that when far from this transition (for example, Fig 2(a) solid line; with surface oxide present) the peak in reflection is a clear peak (peak A). However, as the resonance coincides with it (Fig. 2 (a) dotted line; no surface oxide) the shape of the reflection spectra is affected by it, producing a distinctive spectrum with a strongly broadened peak that displays a drop in reflection in the region of the interband transition (peaks B and C). The influence of the aluminum's optical properties can be observed directly in the dip in normalised reflectance (perpendicular excitation) around 760 nm in Fig. 2(a); this corresponds to a local maximum in the extinction coefficient of the aluminum, which is related to the interband transition at 800 nm.

The numerical simulations in COMSOL Multiphysics enable the visualization of the near-field and surface charge distributions of plasmonic resonances, which provides insight into the nature of the resonances observed experimentally. To reproduce experimental conditions the simulated V-antenna arrays were illuminated with linearly polarized light at normal incidence from the air side of the substrate. The incident light was polarized either parallel or perpendicular to the axis of symmetry of the V (shown schematically in Fig. 1(a), inset). The fields around the antennas were always localized to the particle/SiO<sub>2</sub> interface, as was the surface charge.



**Fig. 3** Simulated normalised absorbance spectra of Aluminum V-antennas on Silicon in 250 nm period arrays compared to the

identical isolated structure for both (a) parallel and (b) perpendicular excitation.

**Perpendicularly polarized excitation:** The perpendicular polarization displayed two resonances at 680 nm and 850 nm, marked as peaks B and C in Fig. 1(b). The surface charge distribution of the 680 nm resonance is shown in the upper inset of Fig. 1(b), and displays a non-dipolar nature. Visualization of the surface charge showed the 850 nm resonance to be a dipole mode with significant localization at the particle/substrate interface, also shown as an inset in Fig. 1(b).

**Parallel polarized excitation:** Modelling suggests weak dipole resonances around 950 nm, 750 nm and 620 nm but all were too weak to be observed experimentally. The experimentally-detected resonance around 520 nm (peak A in Fig. 1(b)) displayed a higher-order, surface charge distribution in simulations, where the surface charge distribution is also shown in Fig. 1(b) as the lower inset.

To gain a greater understanding of the observed modes, identical single V-antennas were also simulated in COMSOL Multiphysics to identify how the antenna resonances are altered when the antennas are part of an array. The single antennas were simulated using the identical unit cell but the x- and y-boundary conditions were altered to scattering boundaries. Incident power then had to account for losses through the scattering boundaries prior to encountering the antennas. For comparison with antennas in arrays the absorption within the antennas due to resistive losses were calculated. To facilitate this comparison each absorption spectra was normalized to incident power and then its peak value. Fig. 3 shows a comparison of the simulated normalized absorption for parallel/perpendicular polarized, normally incident excitation in the upper/lower plots respectively for both single and array antennas. As in previously published work,<sup>35, 36</sup> the additional structure in the absorbance plots is due to an interaction between the LSP modes of the individual particles with coherent multiple scattering from the periodic array. The absorption peaks are slightly red-shifted relative to the simulated and experimental normalised reflectance peaks. Due to interactions with adjacent antennas increasing the field in their near-field environment, the array antennas absorb approximately three times the amount of power as the isolated antenna, although this is not apparent in Fig. 3 due to the normalization process used.

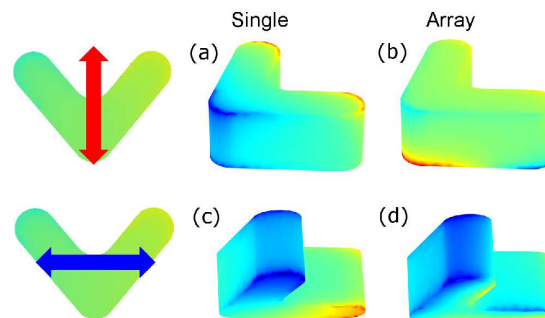


**Fig. 4** Surface charge distributions of an isolated Al V-antenna on silicon substrate at (a) 510 nm (parallel excitation, as defined previously) and (c) 680 nm (perpendicular excitation); and the same antenna in a 250 nm periodic array at (b) 510 nm (parallel excitation) and (d) 680 nm (perpendicular excitation). The different perspectives have been used to differentiate the two wavelengths shown and the assist in highlighting the differences between surface charge distributions. Colour scale is different for each individual

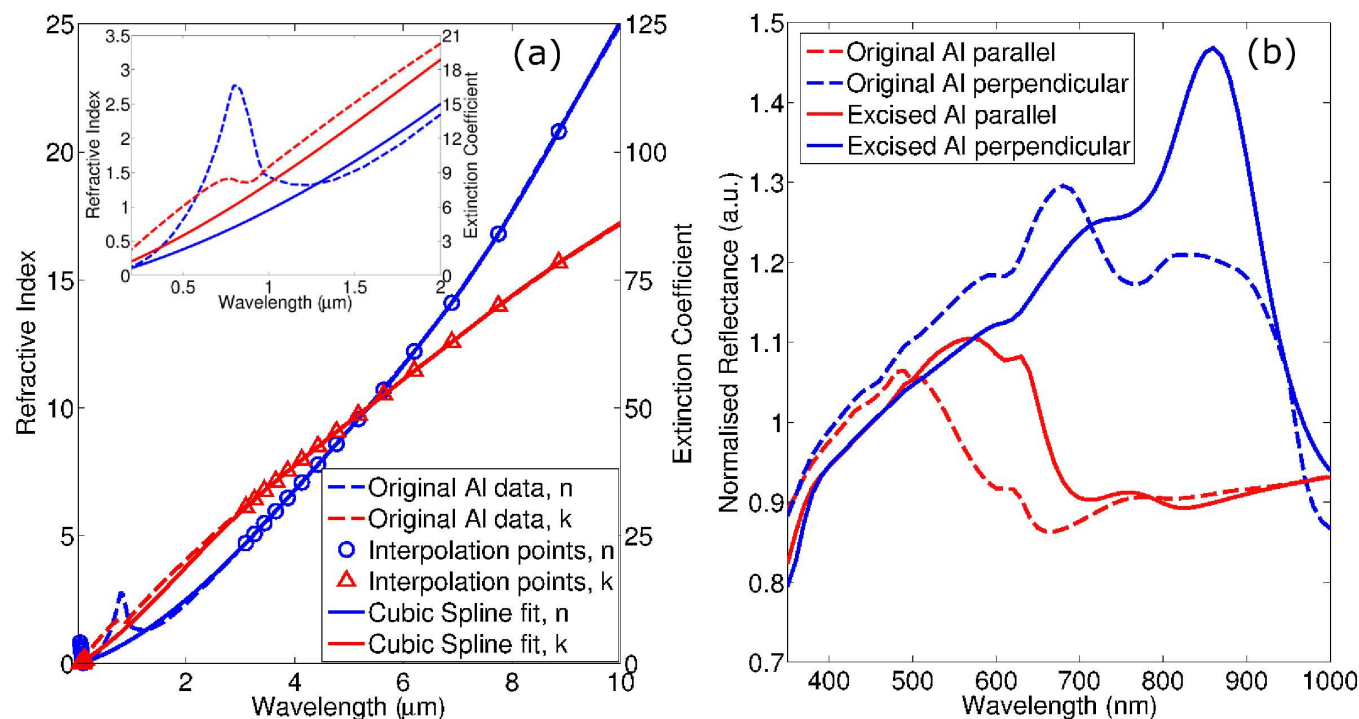


**Fig. 5** (a) Comparison of the original refractive index (blue) and extinction coefficient (red) of aluminum to the data points and cubic spline fit used in the model lacking the 1.5 eV interband transition; (a, inset) Close-up of the region of interest, demonstrating the difference between the actual data and the fitted curve due to the omission of the interband transition; (b) a comparison of FEM results both with (dotted lines) and without (solid lines) the 1.5 eV interband transition.

resonance, with red and blue again indicating opposite charge and green highlighting regions of neutral charge.

Fig. 4 presents a comparison of the surface charge distributions between isolated V-antennas and those in an array for the two higher-order resonances discussed previously to show the effect of the adjacent antennas on the resonant mode. The isolated antenna in both cases displays a dipolar nature, in contrast to those in periodic arrays. This suggests that the LSP resonance's interaction with the grating mode of the array is responsible for the apparent higher-order nature of the parallel/perpendicular resonances located at 510 nm/680 nm in the normalized reflection spectra of Fig. 1(b). Previous work<sup>37-39</sup> has shown that when the spacing between adjacent particles approaches the incident wavelength the extinction spectrum of a particle array is significantly altered as the grating mode switches from radiative to evanescent. Known as Wood's Anomaly this effect has been shown to alter plasmon decay time and extinction spectra,<sup>40</sup> and the wavelengths for which this occurs can be calculated using the grating formula. Assuming perfectly normal incidence and setting the diffraction angle to 90 degrees this simplifies to<sup>40</sup>

$$\frac{m\lambda}{n_{Si}d} = \pm 1, \quad m = \pm 1, \pm 2, \dots$$

where  $m$  is the diffraction order and  $d$  is the periodicity of the array, and where the wavelength of incident light is modified by the refractive index of the silicon substrate.

Applying the grating equation for  $m=1$  finds that the 250 nm period of the antenna array is sufficiently small for there to be no Wood's Anomaly over the measured wavelength range, as defined in the spectrum of Fig. 1. However, including the  $m=2$  term (corresponding to an antenna coupling in the far-field to its next-to-nearest neighbor) the grating equation calculates a

Wood's Anomaly at 525 nm. Inspection of Fig. 3(a) shows that the array plasmon peak at 510 nm is blue-shifted relative to the single antenna peak, in accordance with the findings of Lamprecht *et al.*<sup>38</sup> that a plasmon resonance near the wavelength of a Wood's Anomaly may be spectrally shifted due to the grating-LSP interaction.

Finally, to fully comprehend the behavior of the array antennas, the nature of the aluminum itself must be considered. An increased understanding of the impact of the interband transition on aluminum plasmonic structures has the potential to hasten their integration into existing silicon based technologies and creation of new plasmon-based devices operating at shorter wavelengths difficult to access with silver and gold nanostructures. Previous works have observed spectral features around 1.5 eV (near 800 nm) in the permittivity of bulk aluminum which were ascribed to interband transitions.<sup>26, 41</sup> In the numerical modelling presented here these spectral features also appear due to the use of experimental materials data for aluminum.<sup>34</sup>

In order to gain insight into the impact of the interband transition on the plasmonic resonances of the V-antennas, a simulation was performed using an artificially-altered material based on aluminum. The refractive index and extinction coefficients for this simulation were altered to remove any evidence of the interband transition centred at 800 nm. This was achieved by excising the data points in the region around the interband transition from the experimental data of Rakic, and using the in-built cubic spline interpolation function in COMSOL Multiphysics to fit the remaining data points from 0.3 μm to around 10 μm. Previous works have accomplished this using a Drude model for Aluminum.<sup>16</sup> The resulting FEM simulations would be expected to be sensitive to the details of any fit chosen, but this approach permits an investigation of the

consequences of characteristic changes to the optical properties of the metal associated with the interband transition.

The data points used to form the fit are shown in Fig. 5(a), accompanied by the original, unaltered dispersion curve of bulk aluminum and a cubic spline fit. It is worth noting that this fit was performed using MATLAB rather than COMSOL and is shown only as an aid to visualization. The aim of this investigation was purely to highlight the effect the aluminium interband transition has on the resonances of the antenna array. While the interband transition is spectrally located at 800 nm these simulations show that it potentially affects the plasmon resonances of the structure across the entire visible spectrum through its impact on the optical properties of aluminum. The basic fit used here is sufficient for the purpose of identifying the potential consequences on the plasmonic resonances of the interband transition, particularly given the uncertainties associated with the use of the optical properties of bulk aluminium in the investigation of nanoscale structures. The effects within our simulations are discussed below.

The simulated normalised reflectance of the altered and unaltered aluminum V-antenna arrays are presented in Fig. 5(b), highlighting the effect the interband transition has on the plasmon resonances through its influence on the dispersion of aluminum. A comparison of these altered simulations with the original simulations shows significant differences in the simulated optical activity of the antenna arrays. Interestingly, for the case of perpendicularly polarized incident light, the modified aluminum antenna array shows reduced reflectance at 680 nm, instead showing a stronger, narrower peak at 850 nm. This indicates that aluminum structures resonant in the spectral region of the interband transition are significantly affected as expected. The parallel polarization shows the opposite behavior, displaying a red-shift and broadening of its resonance. Again, this is as expected due to the reduction in both the refractive index and extinction coefficient of the resonant material. The reduction of the extinction coefficient reduces material damping and as a result the normalized amplitude is higher for the modified aluminum structures.

The parallel polarization also displays altered behavior even though its resonance is over 200 nm from the interband transition, since the optical properties of aluminum are affected over the entire visible spectrum. Since this axis is not optically-active around the 800 nm transition there is minimal change between the modified and original array simulations there; there is little field enhancement and so minimal material absorption occurring. The inset in Fig. 5(a) highlights the differences between the two simulated materials, showing how the refractive index and extinction coefficient of the aluminum within the visible range would be altered if the interband transition was not present. Within the visible region the extinction coefficient is increased by the interband transition, increasing absorption within the metal, with the refractive index displaying a peak at 800 nm. As a result of this, the parallel polarized resonance of the original aluminum structures at 520 nm is narrowed relative to the modified-aluminum simulations through additional damping near the red end of its plasmon resonance.

Understanding the impact of the 1.5 eV interband transition may be useful in the design of aluminum plasmonics. Knowing that it will broaden resonances around 800 nm and narrow resonances within the blue may aid deliberate manipulation of these behaviors. It should be remembered, however, that this is an artificially adjusted material in these simulations, and that

this short investigation is an attempt only to understand how far across the visible the interband transition's effects reach.

## Conclusions

It is important to investigate the effects of silicon substrates on plasmonic structures to ensure effective integration of plasmonic structures with existing semiconductor technologies. As demonstrated in this work, the presence of the substrate can significantly alter the resonances of the structure, with higher optical density substrates having a stronger influence. We have reported the fabrication and characterization of an aluminum antenna array on a silicon substrate. We present numerical modelling which closely reproduces the experimental spectra of these structures, and use this to demonstrate that the nature, number and amplitude of these LSP resonances has been altered by the high refractive index of the silicon, the near-unavoidable presence of the silicon's native oxide layer and the periodicity of the array. In addition, we achieve good agreement between experiment and simulation without needing to consider the native oxide layer of the aluminum, in contrast with previous studies, hypothesizing that the presence of the dense substrate is the cause of this decrease in sensitivity to dielectric environment.

By considering the interband transition of aluminum around 800 nm we further investigate the behavior of our antenna arrays, finding that the presence of this transition produces narrower resonances in the blue part of the spectrum than would occur were it absent. This mode-modifying phenomenon may have implications for a wide range of applications whose efficiency could benefit from the use of higher-order modes due to their higher Q-factors and susceptibility to their surroundings.

## Acknowledgements

This work was performed in part at the Melbourne Centre for Nanofabrication (MCN) in the Victorian Node of the Australian National Fabrication Facility (ANFF). It has been supported by the Melbourne-Vanderbilt Partnership Grant and by a grant from the Defence Science Institute. This research was also supported under the Australian Research Council's Discovery Projects funding scheme (project numbers DP110100221 and DP110101767) and a Melbourne Centre for Nanofabrication Technical Fellowship.

## Notes and references

<sup>a</sup> School of Physics, The University of Melbourne, Victoria 3010, Australia.

<sup>b</sup> Melbourne Centre for Nanofabrication (MCN), Australian National Fabrication Facility, Clayton, Victoria, 3168, Australia.

<sup>c</sup> CSIRO Material Science & Engineering, Private Bag 33, Clayton, Victoria 3168, Australia.

1. D. W. Pohl, Near field optics seen as an antenna problem, Beijing, China, 1999.
2. L. Novotny and N. van Hulst, *Nat. Photonics*, 2011, **5**, 83-90.
3. M. Knight, H. Sobhani, P. Nordlander and N. Halas, *Science (New York, N.Y.)*, 2011, **332**, 702-704.
4. S. Earl, T. James, T. Davis, J. McCallum, R. Marvel, R. Haglund and A. Roberts, *Optics express*, 2013, **21**, 27503-27508.

5. I. Thomann, B. A. Pinaud, Z. Chen, B. M. Clemens, T. F. Jaramillo and M. L. Brongersma, *Nano letters*, 2011, **11**, 3440-3446.
6. J. Lee, S. Mubeen, X. Ji, G. D. Stucky and M. Moskovits, *Nano letters*, 2012, **12**, 5014-5019.
7. M. D. Malinsky, K. L. Kelly, G. C. Schatz and R. P. Van Duyne, *The Journal of Physical Chemistry B*, 2001, **105**.
8. T. Yamaguchi, S. Yoshida and A. Kinbara, *Thin Solid Films*, 1974, **21**.
9. A. Pinchuk, A. Hilger, G. Von Plessen and U. Kreibig, *Nanotechnology*, 2004, **15**.
10. K. C. Vernon, A. M. Funston, C. Novo, D. E. Gómez, P. Mulvaney and T. J. Davis, *Nano letters*, 2010, **10**, 2080-2086.
11. M. W. Knight, Y. Wu, J. Britt Lassiter, P. Nordlander and N. J. Halas, *Nano letters*, 2009, **9**, 2188-2192.
12. S. Zhang, K. Bao, N. J. Halas, H. Xu and P. Nordlander, *Nano letters*, 2011, **11**, 1657-1663.
13. B. Luk'yanchuk, N. I. Zheludev, S. A. Maier, N. J. Halas, P. Nordlander, H. Giessen and T. C. Chong, *Nature materials*, 2010, **9**, 707-715.
14. W. Yanpeng and N. Peter, *The Journal of Physical Chemistry C*, 2010, **114**.
15. L. J. Sherry, S.-H. Chang, G. C. Schatz, R. P. Van Duyne, B. J. Wiley and Y. Xia, *Nano letters*, 2005, **5**, 2034-2038.
16. O. Lecarme, Q. Sun, K. Ueno and H. Misawa, *ACS Photonics*, 2014, **1**.
17. S.-Y. Chiam, R. Singh, W. Zhang and A. A. Bettiol, *Applied Physics Letters*, 2010, **97**.
18. M. Yang, J. Li, J. Li and X. Zhu, *Chemphyschem : a European journal of chemical physics and physical chemistry*, 2012, **13**, 2573-2577.
19. J. H. Kang, J.-H. Choe, D. S. Kim and Q. H. Park, *Optics express*, 2009, **17**, 15652-15658.
20. K. L. Shuford, S. K. Gray, M. A. Ratner and G. C. Schatz, *Chemical Physics Letters*, 2007, **435**.
21. A. Roberts and L. Lin, *Optical Materials Express*, 2011, **1**, 480-488.
22. J. F. O'Hara, R. Singh, I. Brener, E. Smirnova, J. Han, A. J. Taylor and W. Zhang, *Optics express*, 2008, **16**, 1786-1795.
23. R. Zia, J. A. Schuller, A. Chandran and M. L. Brongersma, *Materials Today*, 2006.
24. X. Zhang, Y. L. Chen, R.-S. Liu and D. P. Tsai, *Reports on progress in physics. Physical Society (Great Britain)*, 2013, **76**, 46401.
25. P. R. West, S. Ishii, G. V. Naik, N. K. Emani, V. M. Shalaev and A. Boltasseva, *Laser & Photonics Reviews*, 2010, **4**.
26. C. Langhammer, M. Schwind, B. Kasemo and I. Zorić, *Nano letters*, 2008, **8**, 1461-1471.
27. I. Zorić, M. Zäch, B. Kasemo and C. Langhammer, *ACS nano*, 2011, **5**, 2535-2546.
28. M. Castro-Lopez, D. Brinks, R. Sapienza and N. F. van Hulst, *Nano letters*, 2011, **11**, 4674-4678.
29. M. W. Knight, L. Liu, Y. Wang, L. Brown, S. Mukherjee, N. S. King, H. O. Everitt, P. Nordlander and N. J. Halas, *Nano letters*, 2012, **12**, 6000-6004.
30. P. M. Schwab, C. Moosmann, M. D. Wissert, E. W.-G. Schmidt, K. S. Ilin, M. Siegel, U. Lemmer and H.-J. Eisler, *Nano letters*, 2013, **13**, 1535-1540.
31. M. W. Knight, N. S. King, L. Liu, H. O. Everitt, P. Nordlander and N. J. Halas, *ACS nano*, 2013.
32. T. D. James, T. J. Davis and A. Roberts, *Optics Express*, 2014.
33. E. D. Palik, *Handbook of Optical Constants of Solids: Index*, Academic press, 1998.
34. A. D. Rakic, A. B. Djurišić, J. M. Elazar and M. L. Majewski, *Applied optics*, 1998, **37**, 5271-5283.
35. B. Auguié and W. L. Barnes, *Physical Review Letters*, 2008.
36. B. Auguié and W. L. Barnes, *Optics letters*, 2009, **34**, 401-403.
37. M. Meier, A. Wokaun and P. F. Liao, *Journal of The Optical Society of America B-optical Physics*, 1985.
38. B. Lamprecht, G. Schider, R. T. Lechner, H. Ditlbacher, J. R. Krenn, A. Leitner and F. R. Aussenegg, *Physical review letters*, 2000, **84**, 4721-4724.
39. N. Félidj, G. Laurent, J. Aubard, G. Lévi, A. Hohenau, J. R. Krenn and F. R. Aussenegg, *The Journal of chemical physics*, 2005, **123**, 221103.
40. V. G. Kravets, F. Schedin and A. N. Grigorenko, *Physical Review Letters*, 2008, **101**.
41. H. Ehrenreich, H. R. Philipp and B. Segall, *Physical Review*, 1963.